Research Square

Preprints are preliminary reports that have not undergone peer review.
They should not be considered conclusive, used to inform clinical practice,
or referenced by the media as validated information.

Electroacupuncture Alleviates Obesity in Mice via IL-33/ST2–ILC2 Axis Activation and Gut Microbiota Modulation

Yu Chen

chenyu@gzucm.edu.cn

The Third Affiliated Hospital, Guangzhou University of Chinese Medicine

Simin Pan

wendi Luo

https://orcid.org/0009-0006-7436-0908

Jingya Zhou

Yunqi Kong

Wanhua Huo

Yue Lu

Jiqiang Li

Jiankun Chen

Article

Keywords: Electroacupuncture; Obesity; White adipose tissue browning; IL-33/ST2 axis; Type 2 innate lymphoid cells; Immunometabolism

Posted Date: November 9th, 2026

DOI: https://doi.org/10.21203/rs.3.rs-10455298/v1

License: This work is licensed under a Creative Commons Attribution 4.0 International License.
Read Full License

Additional Declarations: There is **NO** conflict of interest to disclose

---

Abstract

Background

Obesity represents a global health crisis driven by chronic energy imbalance and excessive white adipose tissue (WAT) expansion. The inducible browning of WAT—characterized by the emergence of thermogenic beige adipocytes expressing uncoupling protein 1 (UCP1)—has emerged as a compelling therapeutic strategy. The interleukin-33 (IL-33)/suppression of tumorigenicity 2 (ST2) axis and its downstream effector, type 2 innate lymphoid cells (ILC2s), are indispensable regulators of adipose tissue immunometabolism and thermogenic programming. Although electroacupuncture (EA) demonstrates clinically relevant anti-obesity effects, whether it precisely targets the local adipose immune microenvironment to drive WAT browning remains entirely undefined.

Objective

This study aimed to determine whether EA alleviates diet-induced obesity by activating the IL-33/ST2-ILC2 axis to promote WAT browning and restore metabolic homeostasis.

Methods

Male SPF mice were fed a high-fat diet (HFD) for eight weeks to establish obesity, followed by four weeks of EA intervention at metabolic-regulatory acupoints (Zhongwan CV12, Tianshu ST25, Zusanli ST36, Sanyinjiao SP6, and Huizong TE7). Comprehensive metabolic phenotyping (body weight, Lee's index, serum lipid profiles, OGTT, and ITT), histopathological evaluation (H&E staining), flow cytometric quantification of adipose immune populations (ILC2s, M1/M2 macrophages), RT-qPCR, Western blot, immunohistochemistry, and 16S rDNA sequencing were performed. To establish causality, an IL-33 pharmacological inhibitor was administered to verify whether the metabolic and browning effects of EA were strictly dependent on this immune pathway.

Results

EA significantly attenuated HFD-induced weight gain, reduced Lee's index, and corrected dyslipidemia. Histologically, EA ameliorated adipose tissue morphology by reducing white adipocyte hypertrophy and intracellular vacuolization, while restoring brown adipocyte morphology with multilocular lipid droplets. EA elevated serum levels of IL-33 and type 2 cytokines. In adipose tissue, EA increased the proportions of ILC2s and M2 macrophages while reducing M1 macrophage infiltration. Molecularly, EA upregulated IL-33 and ST2 expression and restored thermogenic markers and adipogenic regulators, while decreasing white adipocyte expansion markers. Additionally, EA reshaped gut microbiota composition, increasing α-diversity and remodeling phylum- and genus-level bacterial abundances. Critically, IL-33 inhibitor treatment abolished EA-induced weight loss, adipose tissue remodeling, and thermogenic protein upregulation, and partially attenuated its improvements in lipid metabolism and glucose homeostasis, confirming that IL-33 is an indispensable mediator of EA's anti-obesity and browning effects.

Conclusion

These findings identify the IL-33/ST2-ILC2 axis as a definitive neuro-immune-metabolic effector of EA. By bridging somatic neuromodulation with local immune-driven adipose tissue plasticity, this study delineates a novel mechanistic pathway for EA-induced WAT browning and provides a robust biological rationale for the clinical application of EA as a precision immunometabolic therapy for obesity and its associated metabolic sequelae.

1. Introduction

Obesity has reached epidemic proportions globally, representing a profound challenge to public health due to its causal associations with type 2 diabetes, non-alcoholic fatty liver disease, cardiovascular morbidities, and specific malignancies [1–3]. The pathogenesis of obesity is fundamentally driven by a chronic imbalance between energy intake and energy expenditure, culminating in the excessive expansion of white adipose tissue (WAT) [4]. Historically viewed as a passive reservoir for lipid storage, WAT is now recognized as a highly dynamic endocrine and immunometabolic organ. A critical aspect of WAT plasticity is its capacity to undergo "browning" or "beiging"—a process characterized by the inducible emergence of thermogenic beige adipocytes expressing uncoupling protein 1 (UCP1) within WAT depots[5–7]. The activation of beige adipocytes dissipates biochemical energy as heat, thereby augmenting whole-body energy expenditure. Consequently, targeted pharmacological or physiological interventions that stimulate WAT browning have emerged as compelling strategies for the prevention and treatment of obesity and its associated metabolic sequelae.

The regulation of adipose tissue browning is not strictly governed by adrenergic signaling; it is deeply intertwined with the local immune microenvironment[8]. Recent advances in immunometabolism have highlighted the indispensable role of type 2 innate immunity in maintaining adipose tissue homeostasis and driving thermogenic programming[9]. Within this network, group 2 innate lymphoid cells (ILC2s) represent a crucial resident immune population in WAT. Upon activation, ILC2s secrete type 2 cytokines, such as interleukin-5 (IL-5) and interleukin-13 (IL-13), which subsequently promote the proliferation of eosinophils and the polarization of alternatively activated (M2) macrophages, ultimately facilitating the biogenesis of beige adipocytes [10, 11]. The activation of ILC2s in adipose tissue is predominantly governed by the interleukin-33 (IL-33)/suppression of tumorigenicity 2 (ST2) signaling axis[12, 13]. IL-33, an alarmin cytokine released by resident stromal and endothelial cells in response to metabolic or environmental stress, binds to its canonical receptor ST2 expressed on ILC2s. Sustained activation of the IL-33/ST2-ILC2 axis has been shown to be profoundly protective against diet-induced obesity, whereas its impairment exacerbates metabolic dysfunction [14, 15].

In the context of non-pharmacological interventions, electroacupuncture (EA)—a modern therapeutic modality combining traditional acupuncture with electrical stimulation—has garnered substantial empirical support for its efficacy in managing obesity[16] [17]. Both clinical trials and preclinical murine

models have demonstrated that EA can significantly reduce body weight, ameliorate systemic insulin resistance, and improve circulating lipid profiles [18, 19]. Despite these documented clinical benefits, the fundamental mechanistic basis of EA remains a subject of intense investigation. Currently, the majority of mechanistic studies pertaining to EA in obesity have focused heavily on systemic outcomes, such as neuroendocrine modulation of appetite, regulation of gut microbiota, or broad hypoglycemic and hypolipidemic effects [20].

A critical research gap persists regarding the specific cellular and molecular mechanisms through which EA modulates the local tissue microenvironment. While it is increasingly hypothesized that somatic sensory stimulation via EA might orchestrate localized immunometabolic responses, how EA precisely regulates the immune microenvironment of adipose tissue remains largely undefined. More specifically, whether the profound metabolic remodeling induced by EA is contingent upon the activation of the aforementioned "IL-33/ST2-ILC2" axis is entirely unknown. Addressing this gap is imperative, as elucidating the specific neuro-immune-metabolic crosstalk could shift the paradigm of acupuncture research from descriptive systemic observations to precise molecular targeting.

To address this unresolved paradigm, the present study interrogates the neuro-immune mechanisms underlying the anti-obesity effects of EA, focusing explicitly on the adipose tissue microenvironment. We hypothesize that EA alleviates high-fat diet (HFD)-induced obesity in mice by enhancing the local IL-33/ST2 signaling pathway, which subsequently boosts the functional activity of resident ILC2s, thereby promoting WAT browning and restoring energy homeostasis.

To systematically test this hypothesis, we established a diet-induced obesity (DIO) mouse model using a prolonged high-fat diet, followed by a rigorously controlled EA intervention targeting specific acupoints associated with metabolic regulation. The methodology integrates comprehensive systemic metabolic phenotyping (including indirect calorimetry and glucose/insulin tolerance tests) with high-resolution localized analyses. Flow cytometry is employed to quantify the abundance and activation state of ILC2s within the stromal vascular fraction of WAT. Furthermore, histological evaluations, combined with transcriptomic and protein-level quantifications, are utilized to assess the expression dynamics of the IL-33/ST2 axis and classical thermogenic markers (such as UCP1, PRDM16, and PGC-1α). To establish direct causality, targeted functional rescue and depletion experiments—specifically utilizing ST2-neutralizing antibodies or ILC2-deficient murine models—are conducted to verify whether the browning effects of EA are strictly dependent on this specific immune pathway.

The findings of this study are expected to yield significant contributions to both the fields of neuroimmunology and metabolic disease. By identifying the IL-33/ST2-ILC2 axis as a definitive downstream effector of EA, this research not only delineates a novel mechanistic pathway for EA-induced WAT browning but also bridges the conceptual divide between somatic neuromodulation and local immune tissue plasticity. Ultimately, elucidating this precise molecular mechanism will provide a robust biological rationale for the clinical application of EA in metabolic disorders and may uncover

novel synergistic therapeutic targets that combine neurostimulation with immunomodulation for the treatment of obesity.

2. Materials and methods

2.1 Animals and groups

Male specific pathogen-free (SPF) mice, aged 6-8weeks (20–22)g, were purchased from Hunan SJA Laboratory Animal Co., Ltd. Hunan, China (SCXK [xiang]2021-0002). Mice were housed in a SPF grade experimental animal experiments were performed in strict accordance with the National Institutes of Health Guide for the Care and Use of Laboratory Animals. This study was approved by the Experimental Animal Ethics Committee of Guangzhou University of Chinese Medicine (ZYD-2024-116).

In the first set of experiments, the mice were randomly divided into the control, high-fat diet (HFD) group, HFD + EA group, and HFD + SA group. In the second set of experiments, the mice were divided into five groups: control group, HFD group, HFD + EA group, HFD + IL-33 group, HFD + IL-33 + EA group. After successful modeling of obesity in mice, the control group continued to receive a standard diet, while the other groups maintained on a high-fat diet for a total of 9 weeks. mice in the HFD + EA group were given EA stimulation. The limbs of the mice were fixed using a self-made simple immobilization plate. Acupuncture points including Zhongwan (CV12), Tianshu (ST25, bilateral), Zusanli (ST36, bilateral), Sanyinjiao (SP6, bilateral), and Huizong (TE7, bilateral) were selected. Needles were inserted with twisting manipulation using the even reinforcing-reducing method, followed by connection to an EA device (EA therapeutic apparatus, Huatuo SDZ-II). Continuous waves with a frequency of 2 Hz and an intensity of 1 mA were applied, with the intensity adjusted to induce slight local muscle twitching. Each EA session lasted 15 minutes and was administered once daily for 4 consecutive weeks. In the sham EA group, needles were inserted at non-acupoint sites located 1 cun lateral to the selected acupoints (Zhongwan, Tianshu, Zusanli, Sanyinjiao, and Huizong). The EA frequency, duration, and treatment course were the same as those in the EA group.

2.2 Histopathological Evaluation (HE)

At 13 weeks post-modeling, all animals were euthanized using pentobarbital, and epididymal adipose tissues were harvested. For histological evaluation, white adipose tissue (WAT) specimens were fixed in 4% paraformaldehyde, embedded in paraffin, and sectioned at a thickness of 4 μm. The resulting sections were stained with hematoxylin and eosin (H&E). Whole-field adipocyte morphology, cell size, and cell count were then examined under a light microscope.

2.3 Flow Cytometry

Inguinal white adipose tissue was dissected and placed into ice-cold PBS. Digestion solution was prepared at a volume of 10 mL per gram of adipose tissue, containing Liberase TM at a final concentration of 50 μg/mL (1:100 dilution) and DNase I at 1 μg/mL (1:200 dilution). The tissue was transferred to a small petri dish, minced into pieces smaller than 0.5 × 0.5 cm, and digested by static

incubation at 37°C for 1 hour. Immediately after digestion, the tube was placed on ice, and 10 mL of RPMI-1640 medium supplemented with 10% fetal bovine serum (FBS) was added to terminate the enzymatic reaction. The digested tissue suspension was filtered through a 200-mesh cell strainer. The retained tissue fragments were gently mashed using a syringe plunger, and then rinsed with FACs buffer. The resulting cell suspension was collected and centrifuged at 1500 rpm for 10 minutes at 4°C.

After centrifugation, the supernatant was carefully discarded. The cell pellet was resuspended in 7 mL of 30% Percoll. In a separate clean, dry centrifuge tube, 3 mL of 70% Percoll was gently added to the bottom. The 30% Percoll containing the cells was carefully layered on top of the 70% Percoll, taking care not to mix the two layers. Optionally, 1 mL of RPMI-1640 medium could be layered on top. The tube was centrifuged at 800 × g for 30 minutes at room temperature. After centrifugation, the tube was carefully removed without disturbing the separated layers. The lymphocyte layer located between the 30% and 70% Percoll layers was collected using a pipette. The collected cells were washed once with ice-cold buffer. FcR blocking reagent (anti-CD16/32 antibody) was then added, and the cells were incubated for 30 minutes at 4°C. Following incubation, the cells were washed by centrifugation with FACs buffer. The antibody working solution was added, and the cells were incubated for an additional 30 minutes at 4°C in the dark. After a final wash with FACs buffer by centrifugation, the cells were ready for flow cytometric analysis.

2.4 Immunohistochemistry

Paraffin-embedded adipose tissue sections were deparaffinized in xylene and rehydrated through a graded series of ethanol solutions of increasing concentrations. Antigen retrieval was performed by heating the sections in citrate buffer. Endogenous peroxidase activity was blocked by incubation with 10% bovine serum albumin (BSA) for 30 minutes at room temperature. The sections were then incubated overnight at 4°C with the appropriate primary antibody. After washing three times with phosphate-buffered saline (PBS), the sections were incubated with a horseradish peroxidase (HRP)-conjugated secondary antibody for 1 hour at room temperature. Visualization was achieved using diaminobenzidine (DAB) working solution. Finally, the sections were examined under a light microscope (OLYMPUS, Tokyo, Japan).

2.5 Real-time quantitative polymerase chain reaction (RT–qPCR)

Total RNA was extracted from adipose tissue using Trizol reagent. Chloroform was added, and the mixture was vigorously shaken for 15 seconds, followed by incubation at room temperature for 2–3 minutes. After centrifugation at 12,000 × g for 15 minutes at 4°C, the upper aqueous phase was collected, and isopropanol was added. The sample was incubated at room temperature for 10 minutes and then centrifuged at 12,000 × g for 10 minutes at 4°C to precipitate the RNA. The RNA pellet was washed with 75% ethanol, centrifuged for 5 minutes, and the supernatant was discarded. The pellet was air-dried and dissolved in DEPC-treated water. Then, the extracted RNA was reverse transcribed into

cDNA with 4 × EZscript Reverse Transcription Mix II reagent (EZBioscience) and amplified with the Real-Time PCR Detection System according to the manufacturer's instructions.

2.6 Western blot

Adipose tissue samples weighing 50 mg each were placed into corresponding homogenization tubes. For every 50 mg of tissue, RIPA buffer, PMSF, and phosphatase inhibitors were added, followed by mechanical homogenization. The homogenates were transferred to 1.5 mL centrifuge tubes and centrifuged at 12,000 g at 4°C for 30 minutes. After centrifugation, the supernatants were transferred to new tubes. Protein quantification was performed using a BCA protein assay kit, and the samples were mixed with loading buffer at a 1:4 ratio to denature the proteins. Subsequently, the proteins were resolved by SDS-PAGE and electro transferred onto polyvinylidene fluoride (PVDF) membranes. The membranes were blocked with 5% BSA for 2h at room temperature to prevent non-specific binding, followed by overnight incubation with the primary antibody at 4°C. Then, the membranes were incubated with the appropriate secondary antibody for 1 h at room temperature. After three washes, the signals were visualized using an enhanced chemiluminescence (ECL) imaging apparatus.

2.7 16S rDNA

Following the experimental interventions, Fresh fecal samples were collected from the mice and stored at − 80°C for subsequent 16S rDNA amplicon sequencing. A specific fragment of the bacterial 16S rDNA gene was amplified using primers containing adapter and barcode sequences, employing a two-round PCR strategy. The resulting PCR products were pooled and sequenced on the Illumina NovaSeq 6000 platform (San Diego, CA, USA), targeting the V3–V4 hypervariable regions. The obtained reads were subjected to assembly, quality filtering, denoising, taxonomic annotation, and abundance analysis. These analytical steps allowed for the characterization of the microbial composition of each sample, the identification of compositional differences among groups, and the screening of differentially abundant microbial taxa.

2.8 Statistical analyses

All data are expressed as the mean ± standard error of the mean (SEM). Statistical evaluations were carried out using GraphPad Prism version 9.4.1 (San Diego, USA). Initially, normality testing was applied to all datasets. For data that did not follow a normal distribution, non-parametric tests were employed. In contrast, for normally distributed data, intergroup differences were evaluated using either the Kruskal–Wallis test or analysis of variance (ANOVA). Pairwise group comparisons were performed using Tukey's test or Dunnett's T3 test. A threshold of $P < 0.05$ was set for statistical significance.

3. Results

3.1 EA is effective in preventing HFD-induced weight gain

Body weight and Lee index are shown in Fig. 1A-D. After a 8-week induction period, mice in both the HFD, HFD + SA and HFD + EA groups were 20% heavier than their initial weight before modeling, indicating the successful modeling of all mice in these groups. Following the 5-week EA intervention, the body mass and Lee index of obese mice were significantly reduced, furthermore, at the end of the experiment, the body mass and weight gain of mice in the HFD group were significantly higher than those groups.

3.2 Effects of EA on serum lipid profiles in HFD-fed mice

As shown in Fig. 1E, compared with the Control group, the HFD group exhibited significantly elevated levels of TG, TC, and LDL-C, along with a significantly reduced HDL-C level. In contrast, relative to the HFD group, treatment with HFD + EA significantly decreased serum TG, TC, and LDL-C levels and increased the HDL-C level.

3.3 Histological assessment of adipose tissue morphology by hematoxylin and eosin staining

HE staining revealed that in the Control group, adipocytes exhibited moderate cell size and intracellular vacuole content, with evenly distributed cells, regular structure, and clear cell boundaries. In the HFD group, white adipocytes showed a marked increase in cell volume, displaying a large vacuolated appearance; brown adipocytes also exhibited enlarged cell size with increased intracellular vacuole content, presenting a “whitening” phenotype. In contrast, the HFD + EA group demonstrated a notable improvement in adipose tissue morphology, as evidenced by a significant reduction in white adipocyte size and intracellular vacuole volume, while brown adipocytes appeared nearly restored to a normal state with numerous small intracellular lipid droplets scattered throughout the cytoplasm.

3.4 Effects of EA on serum levels of IL-4, IL-5, IL-13, and IL-33

IL-4, IL-5, IL-13, and IL-33 are all cytokines with anti-inflammatory and immunomodulatory functions. In addition to its immunomodulatory role, IL-33 acts as an alarmin and has been shown to promote thermogenesis and energy metabolism in adipose tissue. The restoration of its levels suggests that EA may ameliorate both metabolic inflammation and energy homeostasis. As shown in Fig. 2A, compared with the Control group, the HFD group exhibited significantly decreased serum levels of IL-4, IL-5, IL-13, and IL-33. In contrast, relative to the HFD group, treatment with HFD + EA significantly elevated the serum levels of these cytokines.

3.5 EA ameliorates adipose tissue dysfunction by modulating gene and protein expression

As shown in Figs. 2B-C, the mRNA expression levels of TMEM26 and CD137 were significantly higher in the HFD group than in the Control group, whereas EA treatment significantly reduced their expression in HFD-fed mice with phlegm-dampness syndrome.

Furthermore, as presented in Figs. 2D-G, the mRNA levels of PPAR-γ, C/EBP-α, LPL, and aP2 were markedly decreased in the HFD group compared with the Control group, and EA treatment significantly upregulated these genes in adipose tissue.

In addition, immunohistochemical analysis (Figs. 2H–J) revealed that the protein expression levels of PGC-1α, PPAR-γ, and UCP1 were significantly lower in the HFD group than in the Control group, while EA treatment markedly elevated their expression.

Collectively, these results indicate that EA can ameliorate adipose tissue dysfunction by reducing markers of white adipocyte expansion and chronic inflammation, while restoring the expression of key regulators involved in adipogenesis, lipid metabolism, and thermogenesis.

3.6 EA reduces M1 macrophage polarization and increases ILC2 proportion in adipose tissue

As shown in Figs. 3A–C, compared with the Control group, the HFD group exhibited a significantly increased proportion of M1 macrophages ($CD45^+CD68^+CD86^+$) in adipose tissue, while the proportions of M2 macrophages ($CD45^+CD68^+CD163^+$) and ILC2 cells ($Lin^-CD45^+CD90^+CD25^+$) were significantly decreased. In contrast, relative to the HFD group, HFD + EA significantly reduced the proportion of M1 macrophages and elevated the proportions of M2 macrophages and ILC2 cells. Collectively, these findings indicate that EA treatment attenuates M1 macrophage polarization and increases ILC2 cell proportion in adipose tissue of obese mice with phlegm-dampness syndrome.

3.7 EA upregulates IL-33 and ST2 expression in adipose tissue

Immunohistochemical staining (Figs. 4A, B) demonstrated that HFD + EA treatment significantly increased the expression levels of both IL-33 and ST2 in adipose tissue. Taken together, these findings indicate that EA can enhance the IL-33/ST2 signaling pathway in adipose tissue.

3.8 EA reshapes gut microbiota composition and structure in HFD-fed mice

To characterize the gut microbiota, we assessed α-diversity using several classical indices including Observed species, Shannon, Chao1, and ACE(Fig. 5A). Compared with the Control group, the HFD group exhibited decreased Observed species, Shannon, Chao1, and ACE indices; conversely, the HFD + EA group showed elevated levels of all these indices compared with the HFD group, suggesting that the therapeutic effects of EA extend beyond overall restoration of microbiota diversity. Principal coordinate analysis (PCoA) was performed based on distance matrices to extract major eigenvectors and reduce high-dimensional community data into two- or three-dimensional space, wherein closer distances between samples indicate greater similarity in species composition. As shown in the Fig. 5B, the EA

group overlapped with and localized near the Control group, indicating highly similar microbiota structures; in contrast, the HFD group was markedly distant from the Control group, suggesting that HFD feeding substantially altered the overall configuration of the gut microbiota.

At the phylum level, analysis of the top 20 most abundant taxa revealed significant differences in microbial composition among the groups (Fig. 5C). Compared with the HFD group, the HFD + EA group exhibited elevated Firmicutes, reduced Bacteroidetes, and a significantly increased Firmicutes-to-Bacteroidetes ratio, indicating that HFD induced marked alterations in gut bacterial community structure at the phylum level.

We further examined the top 20 most abundant genera to profile genus-level bacterial populations (Fig. 5D). Compared with the Control group, HFD-fed mice showed increased relative abundances of *Limosilactobacillus*, *Lactobacillus*, and *Enterococcus* in fecal samples. Compared with the HFD group, the HFD + EA group displayed decreased abundances of *Limosilactobacillus*, *Lactobacillus*, and *Enterococcus*, alongside elevated levels of *Oscillibacter* and *Rikenellaceae*_RC9_gut_group. Collectively, these findings demonstrate that EA reshapes gut microbiota homeostasis in HFD-fed mice through phylum-level ratio remodeling and specific genus-level abundance adjustments.

Correlation analyses revealed that IL-33, ST2, and ILC2 were positively correlated with *Bacteroidota*, while negatively associated with *Firmicutes*, the elevated F/B ratio, and obesity-related genera (Fig. 5E). These findings indicate that EA reshapes gut microbiota composition, reversing HFD-induced dysbiosis to restore IL-33/ST2-mediated ILC2 activation and enhance protective type 2 immune responses, thereby exerting comprehensive anti-obesity effects.

3.9 Pharmacological inhibition of IL-33 abolishes the anti-obesity effects of EA

After 4 weeks of EA intervention combined with IL-33 inhibitor treatment (Fig. 6A, B), the HFD + EA group showed a significant decrease in Lee's index compared with the HFD group ($P < 0.01$). At the end of the experiment, body weight and weight gain in the HFD group were significantly higher than those in the other groups. However, compared with the HFD + IL-33 group, the HFD + IL-33 + EA group exhibited no further reduction in body weight or Lee's index.

Following oral glucose administration (Fig. 6C, D), blood glucose levels in the EA-treated group were significantly lower than those in the HFD group, indicating that HFD + EA treatment ameliorated impaired glucose tolerance in obese mice. After intraperitoneal insulin injection, blood glucose levels in the HFD + EA group were also markedly reduced. Compared with the HFD group, suggesting that HFD + EA treatment alleviated impaired insulin tolerance.

Furthermore, HE staining revealed that white adipocytes in the IL-33 + EA group were markedly enlarged and displayed prominent vacuolated morphology (Fig. 6E), while brown adipocytes showed increased cell size with enhanced intracellular vacuolization, indicative of a phenotypic shift toward whitening.

These results collectively demonstrate that IL-33 is an indispensable mediator of the anti-obesity and adipose-remodeling effects of EA, whereas its improvements in glucose homeostasis and insulin sensitivity occur through an IL-33-independent mechanism.

3.10 IL-33 mediates EA-induced PENK upregulation and lipid metabolic improvement

Meanwhile, we examined PENK expression and serum lipid parameters. As shown in the Fig. 6F, G, compared with the Control group, both the HFD group and the HFD + IL-33 group exhibited significantly decreased PENK expression, accompanied by elevated TG, TC, and LDLC levels and reduced HDLC levels. Compared with the HFD group, HFD + EA group significantly upregulated PENK expression and reversed these dyslipidemia alterations. However, relative to the HFD + EA group, the HFD + IL-33 + EA group showed significantly decreased PENK expression, increased TG, TC and HDLC levels, indicating that IL-33 inhibition partially reverses the therapeutic effects of EA. These results collectively demonstrate that IL-33 is an essential mediator of the beneficial effects of EA on PENK expression and lipid metabolism.

3.11 IL-33-Independent Restoration of ILC2 Proportion by EA

As shown in the Fig. 7A, compared with the control group, the proportion of ILC2s was significantly decreased in both HFD and HFD + IL-33 group. Compared with the HFD group, HFD + EA treatment significantly increased the ILC2 proportion. However, relative to the HFD + EA group, the HFD + IL-33 + EA group exhibited a numerically elevated ILC2 proportion without statistical significance.

3.12 IL-33 Mediates EA-Induced IL-33/ST2 Upregulation

As shown in the Fig. 7B, C, compared with the control group, both HFD and the HFD + IL-33 group showed significantly decreased expression of IL-33 and ST2. Compared with the HFD group, HFD + EA treatment significantly upregulated IL-33 and ST2 expression. However, relative to the HFD + EA group, the HFD + IL-33 + EA group exhibited significantly decreased IL-33 and ST2 expression, indicating that IL-33 inhibition partially reverses the effects of EA.

3.13 IL-33 Mediates EA-Induced Thermogenic protein Upregulation

Immunohistochemical staining revealed that (Fig. 8A-C), compared with the control group, both HFD and the HFD + IL-33 group exhibited significantly decreased expression of PGC-1α, PPAR-γ, and UCP1. Compared with the HFD group, HFD + EA treatment significantly increased the expression of PGC-1α, PPAR-γ, and UCP1. However, relative to the HFD + EA group, the HFD + IL-33 + EA group showed significantly reduced expression of PGC-1α, PPAR-γ, and UCP1, indicating that IL-33 inhibition partially

reverses the effects of EA. These results collectively demonstrate that IL-33 is a critical mediator of EA-induced upregulation of PGC-1α, PPAR-γ, and UCP1.

4.Discussion

These findings identify the IL-33/ST2-ILC2 axis as a definitive neuro-immune-metabolic effector of EA. By bridging somatic neuromodulation with local immune-driven adipose tissue plasticity, this study delineates a novel mechanistic pathway for EA-induced WAT browning and provides a robust biological rationale for the clinical application of EA as a precision immunometabolic therapy for obesity and its associated metabolic sequelae. While traditional perspectives have primarily viewed acupuncture as an autonomic or central nervous system modulator, our data extends this paradigm by establishing a direct peripheral interface where EA recruits type 2 immunity. The concurrent restoration of gut microbiota α-diversity further implies that EA exerts a multi-systemic metabolic reset. Consequently, EA functions not merely as a local symptomatic treatment, but as a comprehensive biological modulator capable of reprogramming systemic energy dissipation and tissue homeostasis without the need for pharmacological intervention.

The present findings align with and extend an expanding body of literature on the metabolic efficacy of EA. Previous studies have established that EA attenuates high-fat-diet-induced weight gain and dyslipidemia through intracellular signaling hubs such as the PKA/CREB and AMPK pathways, which promote mitochondrial biogenesis and thermogenic gene expression in adipose tissue[21]. Our results complement this molecular framework by demonstrating that these metabolic benefits are critically gated by the IL-33/ST2–ILC2 immunological axis. This converges with reports that endogenous IL-33 deficiency exacerbates adiposity and insulin resistance, whereas IL-33 administration expands adipose-resident ILC2s and drives beige adipogenesis via type 2 cytokine production[22, 23]. The observed shift from M1 to M2 macrophage polarization further resonates with evidence that EA modulates neuro-immune crosstalk to suppress chronic low-grade inflammation, likely through ILC2-directed type 2 signaling that precedes and orchestrates macrophage reprogramming[24]. Additionally, the remodeling of gut microbiota—characterized by increased diversity and altered phylum-level abundances—is consistent with recent studies showing that EA restores beneficial taxa and reduces metabolic endotoxemia in obese rodents [25].

An intriguing nuance in our findings was the incomplete reversal of metabolic parameters during IL-33 blockade. While the pharmacological inhibition of IL-33 entirely abolished EA-induced weight loss, adipose tissue morphological remodeling, and thermogenic marker expression, it only partially attenuated the improvements in systemic lipid and glucose homeostasis. This divergence suggests that EA's regulatory network is highly pleiotropic. It is highly probable that while the morphological browning of WAT is strictly dependent on the IL-33/ST2-ILC2 axis, systemic glucose disposal and lipid clearance are simultaneously managed by parallel, IL-33-independent pathways. For instance, EA has been shown to directly enhance skeletal muscle glucose uptake via AMPK activation and modulate hepatic lipid

metabolism through vagal efferent signaling[26]. Additionally, the reshaped gut microbiota may independently contribute to glycemic control via the production of short-chain fatty acids (SCFAs), which bypass local adipose immune requirements to systematically enhance insulin sensitivity[20].

Despite the mechanistic insights provided, several limitations must be acknowledged. First, translating neuro-immune-metabolic interactions from murine high-fat diet models to the complex heterogeneity of human obesity requires caution, as species-specific differences in ILC2 distribution and basal metabolic rates are significant[27]. Second, our reliance on a pharmacological IL-33 inhibitor introduces the possibility of off-target effects and systemic variations that genetic knockout models could circumvent. Third, although we observed robust reshaping of the gut microbiota composition following EA, the cross-sectional nature of this sequencing lacks Fecal Microbiota Transplantation (FMT) validation. Therefore, it remains undetermined whether the altered microbiota actively drives the observed metabolic improvements or merely reflects a secondary consequence of the overall reduction in adiposity.

Future investigations should systematically address these mechanistic gaps to fully map the EA-induced therapeutic network. The precise neural circuitry—from the primary somatosensory afferents activated by EA to the efferent pathways controlling localized IL-33 release—remains a critical black box[28]. Moreover, incorporating conditional ST2 knockout mice and FMT experiments will provide definitive causality regarding the immune and microbial drivers of EA efficacy[29]. Clinically, longitudinal human trials are warranted to investigate whether peripheral fluctuations in IL-33, ILC2 populations, and specific bacterial taxa can serve as viable, non-invasive biomarkers to monitor and predict patient responsiveness to EA interventions in obesity management. Circulating IL-33 levels are significantly associated with metabolically unhealthy obesity phenotypes and cardiometabolic risk factors [30]. Adipose-resident ILC2s are critical mediators of IL-33-driven white adipose tissue browning and energy expenditure[31]. The demonstration that IL-33 treatment expands ILC2 populations in adipose tissue to promote beiging and limit adiposity underscores their potential clinical relevance [32].

5. Conclusion

In conclusion, this study establishes a neuro-immuno-metabolic framework for EA mediated anti-obesity effects. In HFD-fed mice, EA significantly reduced adiposity, improved serum lipid profiles, and ameliorated hepatic steatosis by activating the IL-33/ST2 axis to expand adipose-resident ILC2s and upregulate browning markers thereby promoting white adipose tissue beiging. Concurrently, EA reshaped gut microbiota composition, restoring the Firmicutes-to-Bacteroidetes ratio and modulating specific bacterial genera. These findings reveal a molecular relay whereby somatosensory stimulation triggers IL-33 release and ILC2-driven adipose remodeling. Clinically, EA represents a viable non-pharmacological obesity intervention, with peripheral IL-33, ILC2 dynamics, and signature bacterial taxa serving as promising biomarkers for predicting patient responsiveness. This work integrates classical acupuncture theory with contemporary immunometabolism and microbiome science, providing an

evidence-based rationale for incorporating EA into precision medicine frameworks for metabolic disease management.

Declarations

Declaration of Interest□Competing Interests□

The authors declare no conflict of interest.

Funding□ Acknowledgements□

This work was supported by grants from the Natural Science Foundation of Guangdong Province (2024A1515012133), the State Key Laboratory of Dampness Syndrome of Chinese Medicine Special Fund (SZ2021ZZ08), the Guangdong Provincial Bureau of Chinese Medicine (20254058□20241147□ 20261141), the Guangdong Provincial Hospital of Chinese Medicine Fund (YN2024GZRPY044, YN2024MS034, YN2025TS036, ZH2025ZJPY10□ZH2025ZJYF04).

Authors' contributions

Simin Pan performed experiments and wrote the article. Wendi Luo and Jingya Zhou contributed to construction and treatment of mice model. Yunqi Kong and Wanhua Huo contributed to the acquisition and analysis of data. Yue Lu, Jiqiang Li, Jiankun Chen, and Yu Chen contributed to the design of study and punishment of article.

References

1. Obesity LINXLIH (2021) Epidemiology, Pathophysiology, and Therapeutics [J]. Front Endocrinol (Lausanne) 12:706978
2. BLÜHER M (2019) Obesity: global epidemiology and pathogenesis [J]. Nat Rev Endocrinol 15(5):288–298
3. POWELL-WILEY TM (2021) Obesity and Cardiovascular Disease: A Scientific Statement From the American Heart Association [J]. Circulation 143(21):e984–e1010
4. ROSEN E. D., SPIEGELMAN B. M. What we talk about when we talk about fat [J]. Cell, (2014) 156(1–2): 20–44
5. COHEN P., KAJIMURA S. The cellular and functional complexity of thermogenic fat [J]. Nat Rev Mol Cell Biol, (2021) 22(6): 393–409
6. WANG W (2016) Control of brown and beige fat development [J]. Nat Rev Mol Cell Biol 17(11):691–702

7. JI X., ZHANG X., ZHANG T., et al. PNPLA7 mediates Parkin-mitochondrial recruitment in adipose tissue for mitophagy and inhibits browning [J]. Nat Commun, (2025) 16(1): 6651
8. LI J., LV Z., FAN Q., et al. The immunoregulatory effect of short-chain fatty acids in type 2 diabetes mellitus [J]. Front Nutr, (2026) 13: 1807302
9. KLOSE C. S., ARTIS D. Innate lymphoid cells as regulators of immunity, inflammation and tissue homeostasis [J]. Nat Immunol, (2016) 17(7): 765–774
10. KLEIN CARDOSOF (2021) Neuro-mesenchymal units control ILC2 and obesity via a brain-adipose circuit [J]. Nature 597(7876):410–414
11. BANDO J. K., COLONNA M. Innate lymphoid cell function in the context of adaptive immunity [J]. Nat Immunol, (2016) 17(7): 783–789
12. LO J. W., SCHROEDER J. H., ROBERTS L. B., et al. CTLA-4 expressing innate lymphoid cells modulate mucosal homeostasis in a microbiota dependent manner [J]. Nat Commun, (2024) 15(1): 9520
13. PASTILLE E., WASMER M. H., ADAMCZYK A., et al. The IL-33/ST2 pathway shapes the regulatory T cell phenotype to promote intestinal cancer [J]. Mucosal Immunol, (2019) 12(4): 990–1003
14. SUN J., ZHANG Y., ZHANG Q., et al. Metabolic regulator LKB1 controls adipose tissue ILC2 PD-1 expression and mitochondrial homeostasis to prevent insulin resistance [J]. Immunity, (2024) 57(6): 1289 – 305.e9.
15. LAN ZHEN, QING HUANG, GUILIN ZHAO et al (2025) The role of adipose tissue-resident immune cells in the occurrence and development of obesity [J]. Mod Immunol 45(03):324–327
16. DING L., TENG R., ZHU Y., et al. Electroacupuncture treatment ameliorates metabolic disorders in obese ZDF rats by regulating liver energy metabolism and gut microbiota [J]. Front Endocrinol (Lausanne), (2023) 14: 1207574
17. GAO H., TONG X., HU W., et al. Three-dimensional visualization of electroacupuncture-induced activation of brown adipose tissue via sympathetic innervation in PCOS rats [J]. Chin Med, (2022) 17(1): 48
18. LI X., LIN J., HU C., et al. Effect and safety of electroacupuncture on weight loss in obese patients with pre-diabetes: study protocol of a randomised controlled trial [J]. BMJ Open, (2024) 14(3): e075873
19. WANG M. N., ZHAI M. X., WANG Y. T., et al. Mechanism of Acupuncture in Treating Obesity: Advances and Prospects [J]. Am J Chin Med, (2024) 52(1): 1–33
20. XIA X., XIE Y., GONG Y., et al. Electroacupuncture promoted intestinal defensins and rescued the dysbiotic cecal microbiota of high-fat diet-induced obese mice [J]. Life Sci, (2022) 309: 120961
21. LIAO C., TANG C. L., QIU W., et al. [Electroacupuncture activates PKA / CREB signaling pathway to promote browning of white fat in obese rats] [J]. Zhen Ci Yan Jiu, (2025) 50(5): 553–566
22. RANA B. M. J., JOU E., BARLOW J. L., et al. A stromal cell niche sustains ILC2-mediated type-2 conditioning in adipose tissue [J]. J Exp Med, (2019) 216(9): 1999–2009

23. LIN Y., XIAO L., CAI Q., et al. The chemerin-CMKLR1 axis limits thermogenesis by controlling a beige adipocyte/IL-33/type 2 innate immunity circuit [J]. Sci Immunol, (2021) 6(61)
24. D'CRUZ DWYERGK (2022) Emerging Functions of IL-33 in Homeostasis and Immunity [J]. Annu Rev Immunol 40:15–43
25. SI Y. C., REN C. C., ZHANG E. W., et al. Integrative Analysis of the Gut Microbiota and Metabolome in Obese Mice with Electroacupuncture by 16S rRNA Gene Sequencing and HPLC-MS-based Metabolic Profiling [J]. Am J Chin Med, (2022) 50(3): 673–690
26. JIA X., LI M., ZHANG W., et al. Adjusting internal organs and dredging channelon electroacupuncture glycolipid metabolism disorders in NAFLD mice by mediating the AMPK/ACC signaling pathway [J]. Diabetol Metab Syndr, (2024) 16(1): 173
27. SASAKI T., MORO K., KUBOTA T., et al. Innate Lymphoid Cells in the Induction of Obesity [J]. Cell Rep, (2019) 28(1): 202 – 17.e7.
28. LIU S., WANG Z., SU Y., et al. A neuroanatomical basis for electroacupuncture to drive the vagal-adrenal axis [J]. Nature, (2021) 598(7882): 641–645
29. OKAMURA T., HASHIMOTO Y., MORI J., et al. ILC2s Improve Glucose Metabolism Through the Control of Saturated Fatty Acid Absorption Within Visceral Fat [J]. Front Immunol, (2021) 12: 669629
30. A M., WANG G., ZAMMIT N. W., et al. Irisin ameliorates obesity and insulin resistance via adipose tissue IL-33 and regulatory T cells [J]. Nat Metab, (2026) 8(4): 885–901
31. OLGUÍN-MARTÍNEZ E., RUIZ-MEDINA B. E., LICONA-LIMÓN P (2021) Tissue-Specific Molecular Markers and Heterogeneity in Type 2 Innate Lymphoid Cells [J]. Front Immunol 12:757967
32. KABAT A. M., HACKL A., SANIN D. E., et al. Resident T(H)2 cells orchestrate adipose tissue remodeling at a site adjacent to infection [J]. Sci Immunol, (2022) 7(76): eadd3263

Figures

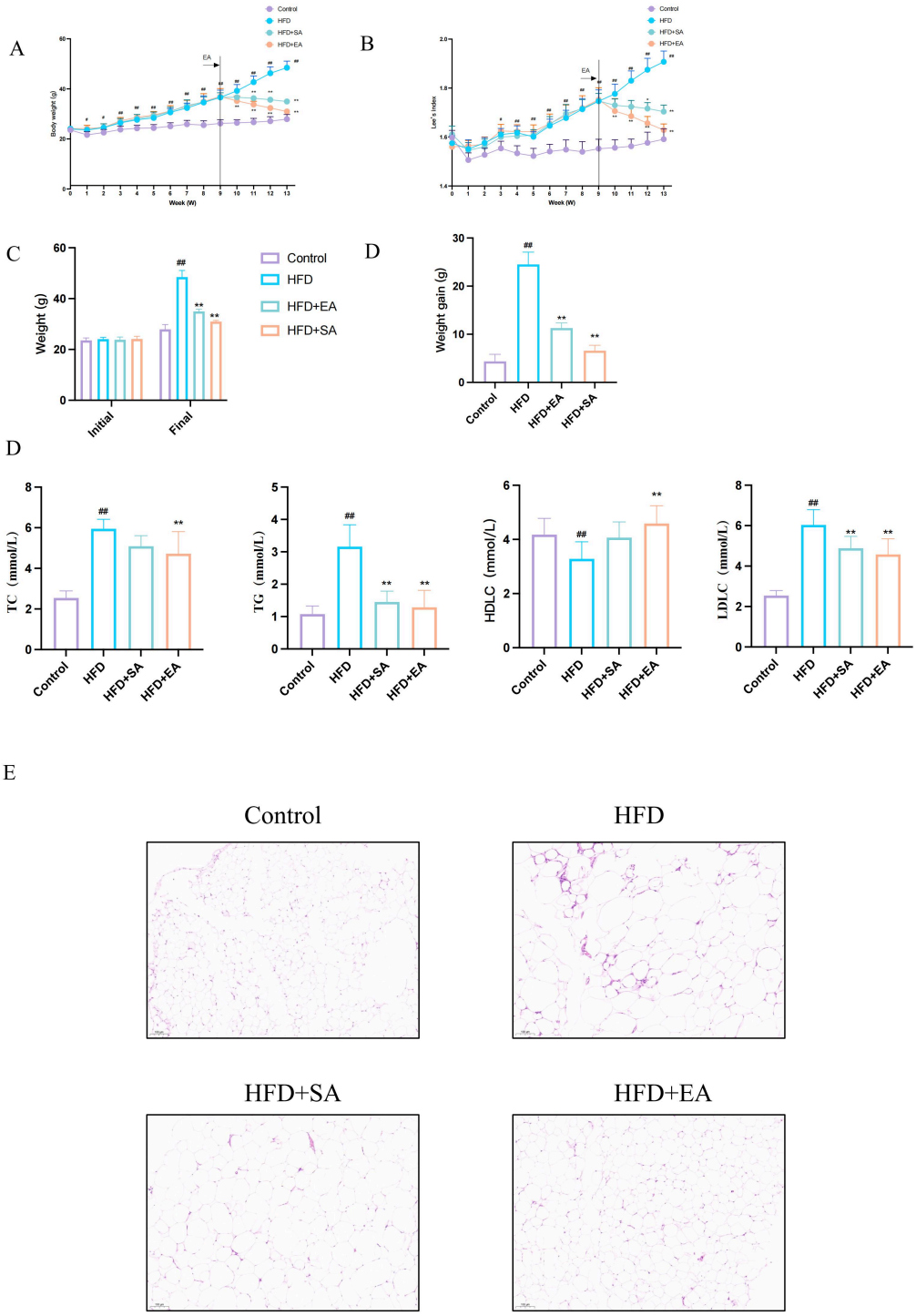


Figure 1

EA attenuates HFD-induced obesity, dyslipidaemia, and adipose tissue whitening in mice. (A) Body weight in grams over 13-week study. (B) Lee index over 13-weeks study. (C) Body weight of mice at beginning and end of 13-week study. (D) Body weight gain in grams over 13-week study. (E) Serum lipid profiles in HFD-fed mice. (F) HE staining of WAT adipocyte size (200×). $^{\#}P < 0.05$, $^{\#\#}P < 0.01$ vs. the control group. $^{*}P < 0.05$, $^{**}P < 0.01$ vs. the HFD group;(n=8).

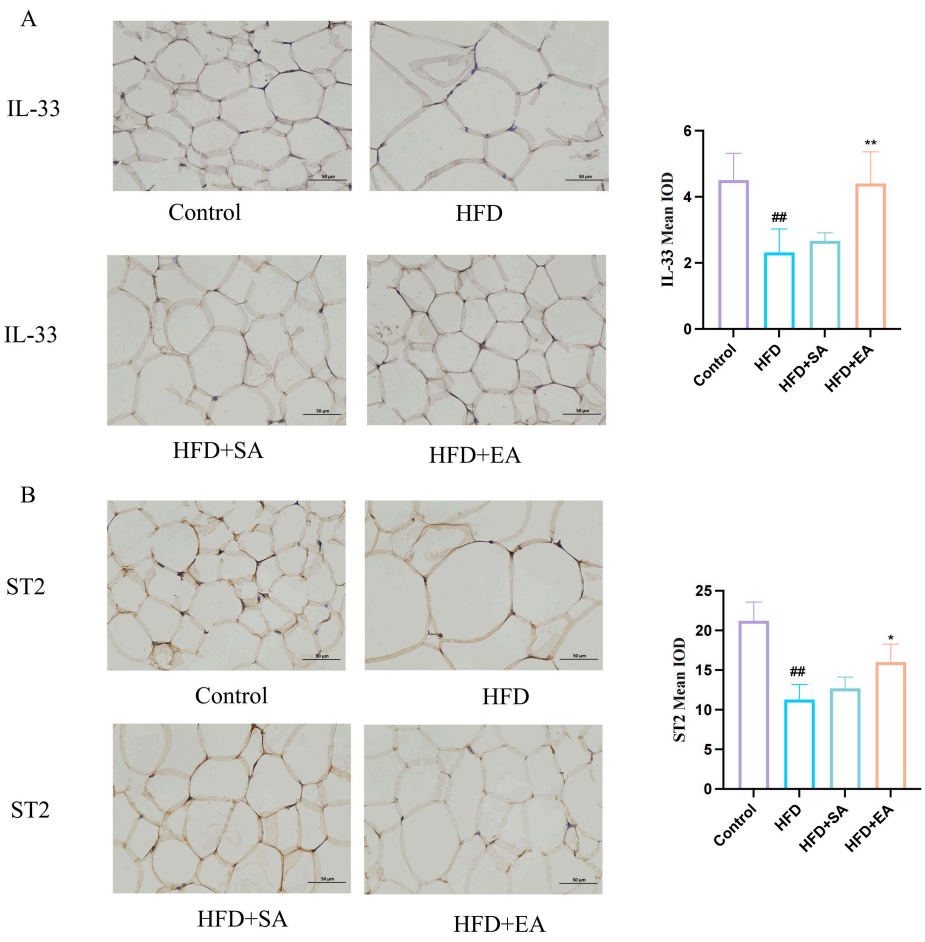


Figure 2

EA upregulates IL-33 and ST2 expression in adipose tissue. (A) Expression of IL-33 and (B) ST2 evaluated by immunohistochemical. $^{\#}P < 0.05$, $^{\#\#}P < 0.01$ vs. the control group. $^{*}P < 0.05$, $^{**}P < 0.01$ vs. the HFD group; (n=3-6).

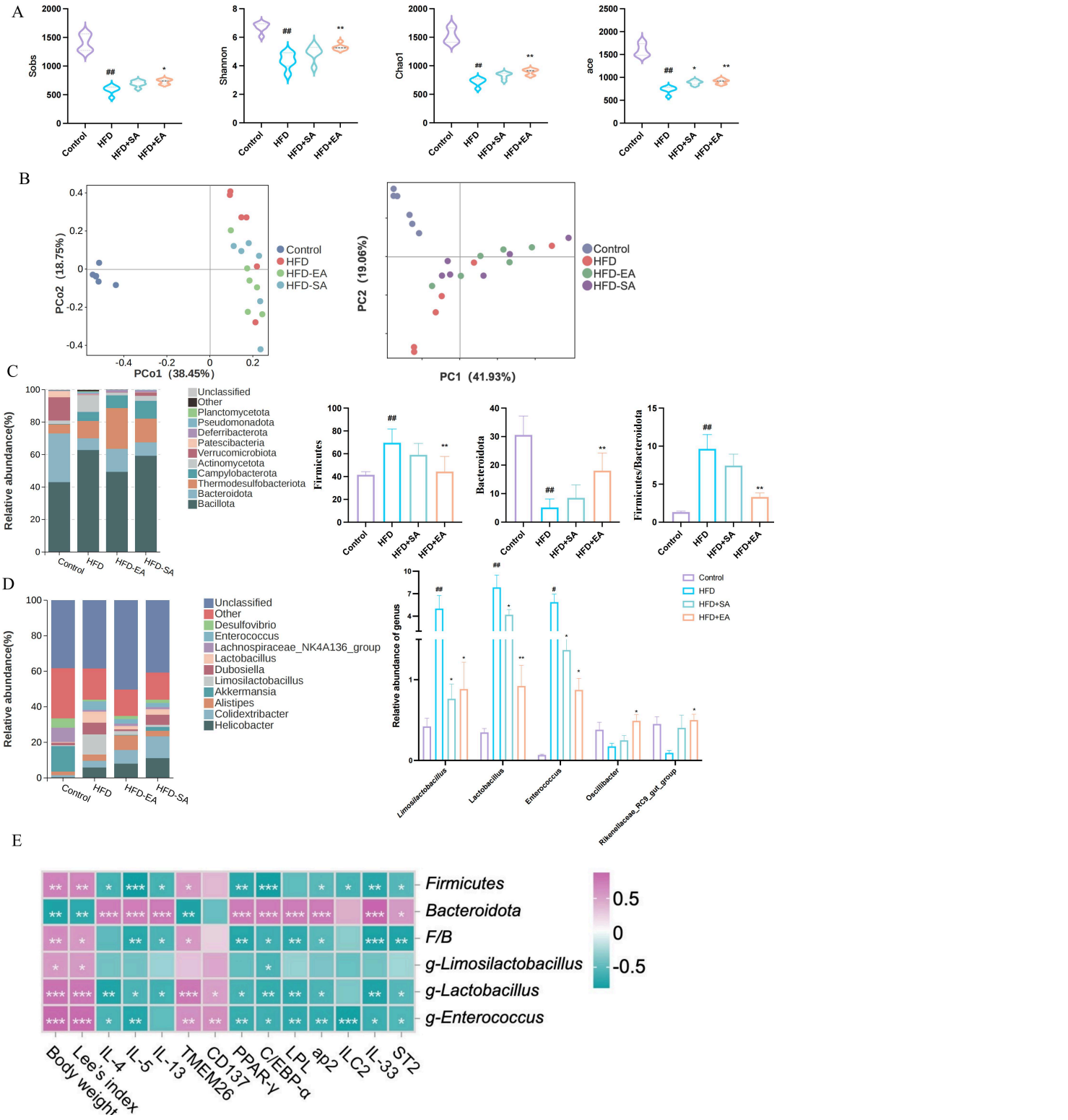


Figure 3

EA reshapes gut microbiota composition and structure in HFD-Fed mice. (A) α-diversity analysis of gut bacterial richness. (B) PCoA analysis of intestinal flora. (C) Community structure analysis at the phylum level. (D) Community structure analysis at the genus level and relative abundance of the genus levels. (E) Heat map of correlation analysis. $^{\#\#}P < 0.01$ vs. the control group. $^{*}P < 0.05$, $^{**}P < 0.01$ vs. the HFD group; (n=6).

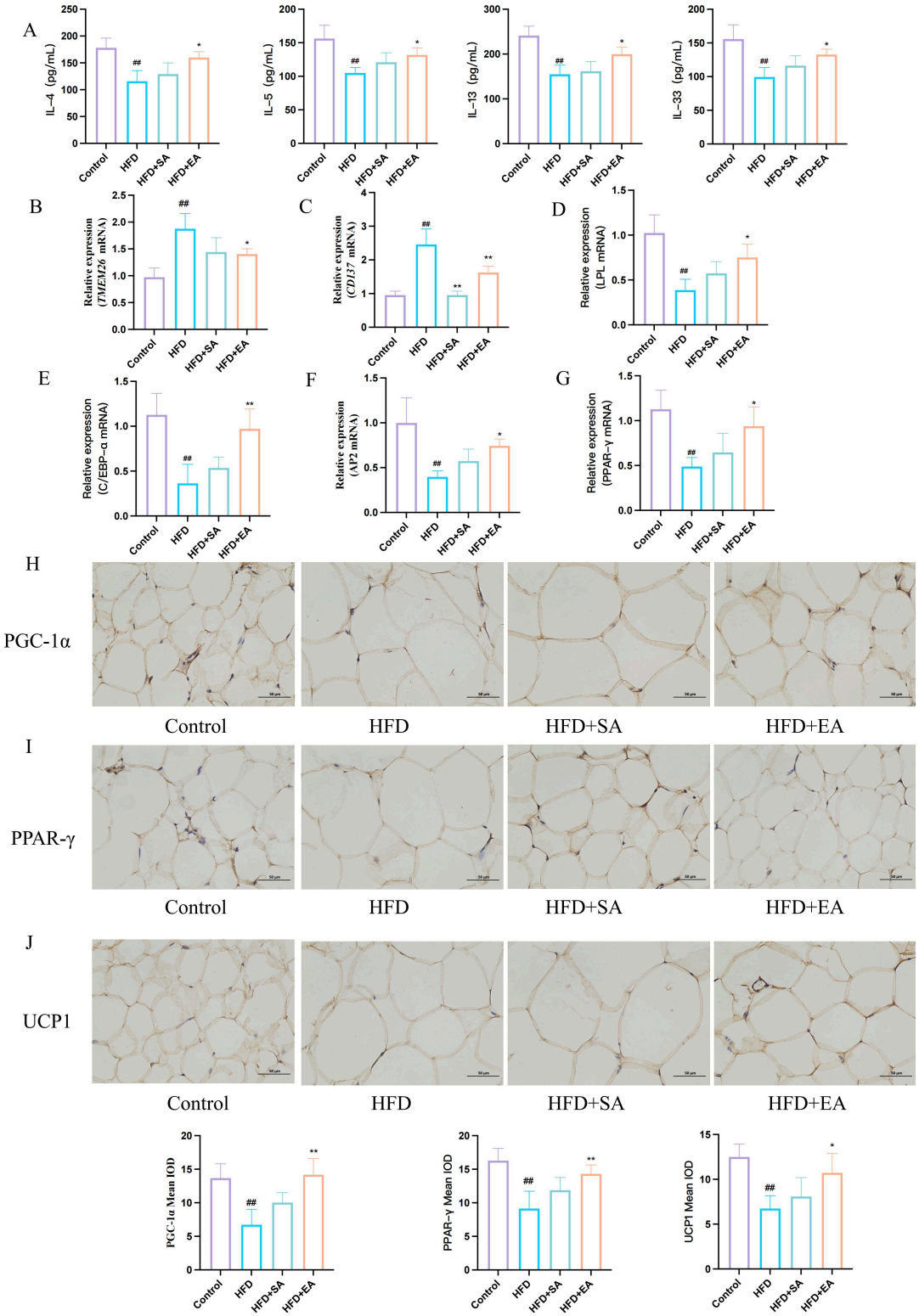


Figure 4

EA attenuates HFD-induced obesity, dyslipidaemia, and adipose tissue whitening in mice. (A) Serum levels of IL-4, IL-5, IL-13, and IL-33. (B-C) mRNA expression levels of TMEM26 and CD137. (D-G) the mRNA levels of PPAR-γ, C/EBP-α, LPL, and aP2. (H-I) Expression of PGC-1α, PPAR-γ and UCP1 evaluated by immunohistochemical. $^{\#}P < 0.05$, $^{\#\#}P < 0.01$ vs. the control group. $^{*}P < 0.05$, $^{**}P < 0.01$ vs. the HFD group;(n=4).

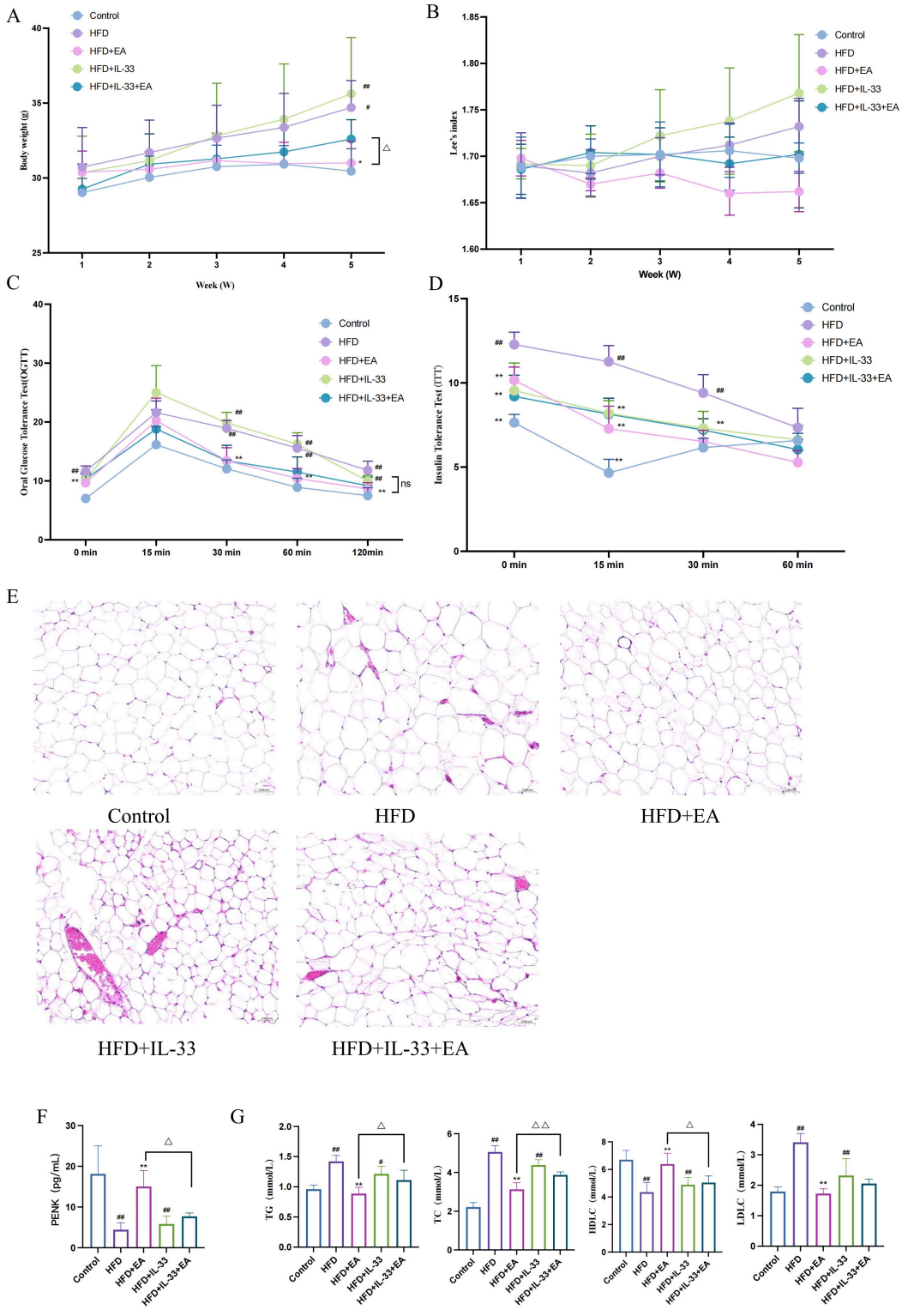


Figure 5

Pharmacological inhibition of IL-33 abolishes the anti-obesity effects of EA. (A) Body weight of mice in each group. (B) Lee index of mice in each group. (C) OGTT Oral glucose tolerance test (OGTT) of mice in each group. (D) Insulin Tolerance Test (ITT) of mice in each group. (E) HE staining of WAT adipocyte size (200×). (F) Serum levels of PENK. (G) Serum lipid profiles in HFD-fed mice. $^{\#}P < 0.05$, $^{\#\#}P < 0.01$ vs. the control group. $^{*}P < 0.05$, $^{**}P < 0.01$ vs. the HFD group; $^{\triangle}P < 0.05$, $^{\triangle\triangle}P < 0.01$, vs. the HFD+EA group (n=5).

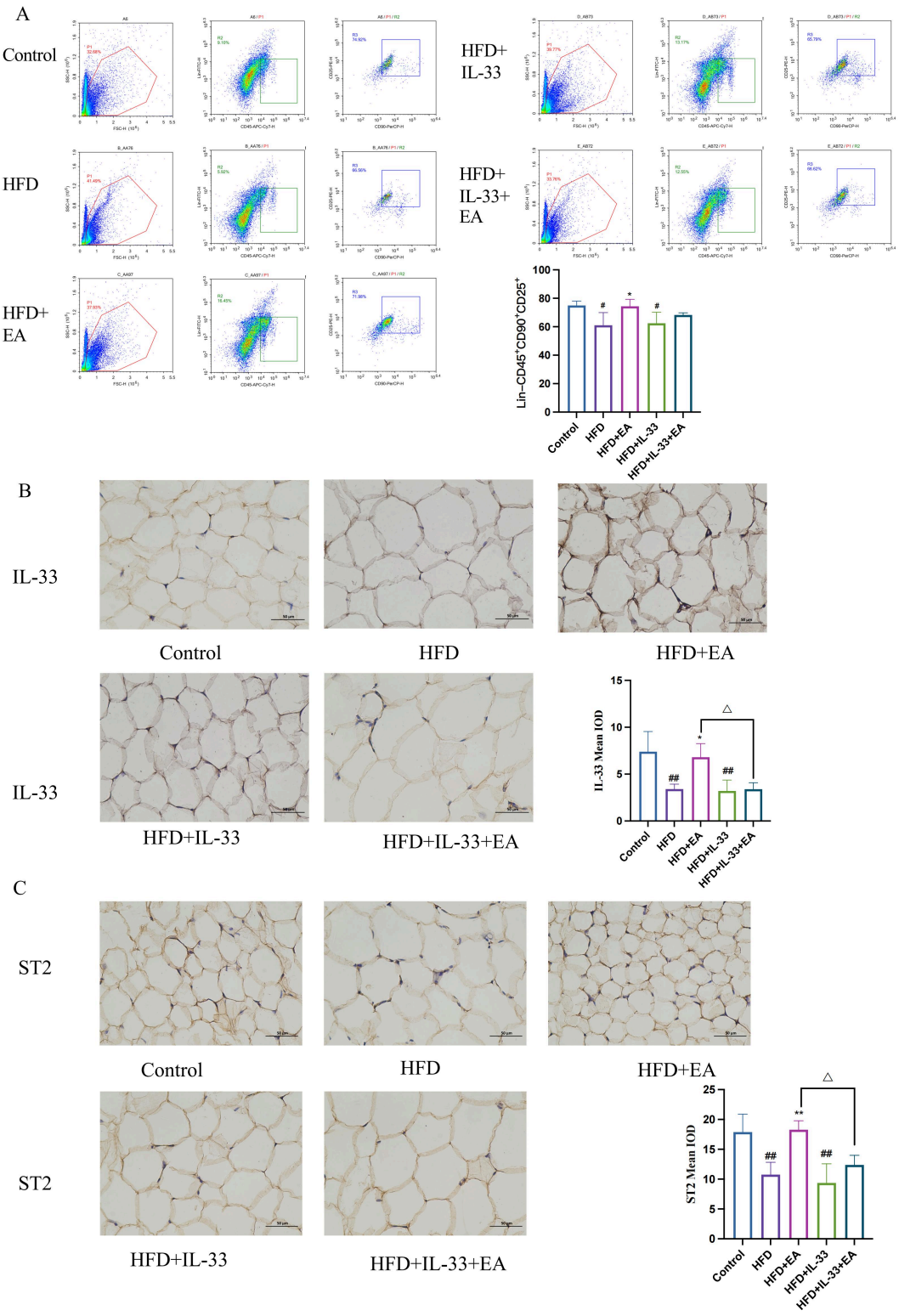


Figure 6

EA therapy regulates the proportion of ILC2 cells by acting through the IL-33/ST2 pathway. (A) The proportions of ILC2 cells ($Lin^{-}CD45^{+}CD90^{+}CD25^{+}$). (B) Expression of IL-33 and (C) ST2 evaluated by immunohistochemical. $^{\#}P < 0.05$, $^{\#\#}P < 0.01$ vs. the control group. $^{*}P < 0.05$, $^{**}P < 0.01$ vs. the HFD group; $^{\triangle}P < 0.05$, $^{\triangle\triangle}P < 0.01$, vs. the HFD+EA group (n=4-5).

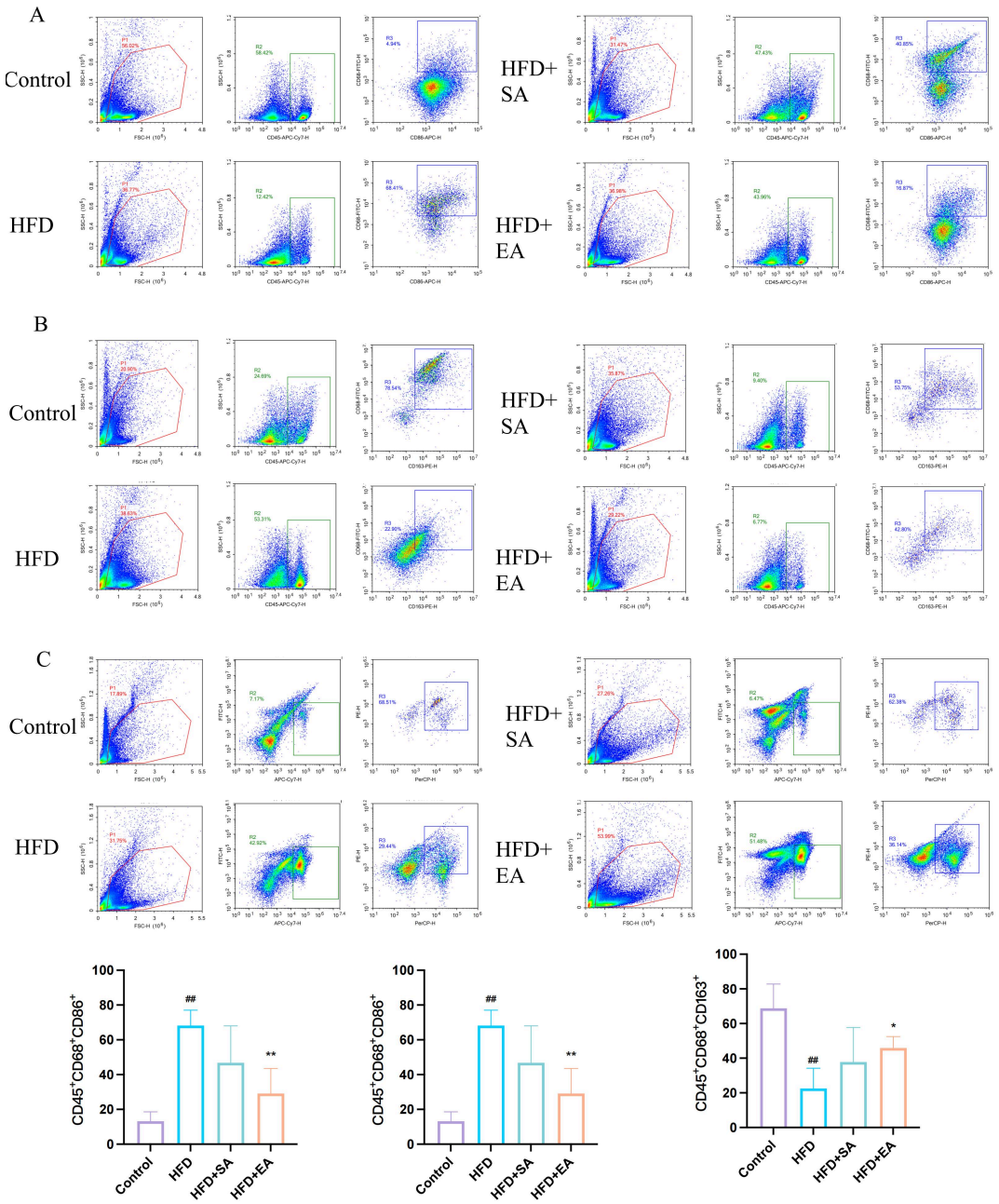


Figure 7

EA reduces M1 macrophage polarization and increases ILC2 proportion in adipose tissue. (A) The proportion of M1 macrophages ($CD45^+CD68^+CD86^+$) in adipose tissue. (B) The proportions of M2 macrophages ($CD45^+CD68^+CD163^+$) (C) The proportions of ILC2 cells ($Lin^-CD45^+CD90^+CD25^+$). $^{\#\#}P <$ 0.01 vs. the control group. $^{*}P < 0.05$, $^{**}P < 0.01$ vs. the HFD group;(n=6).

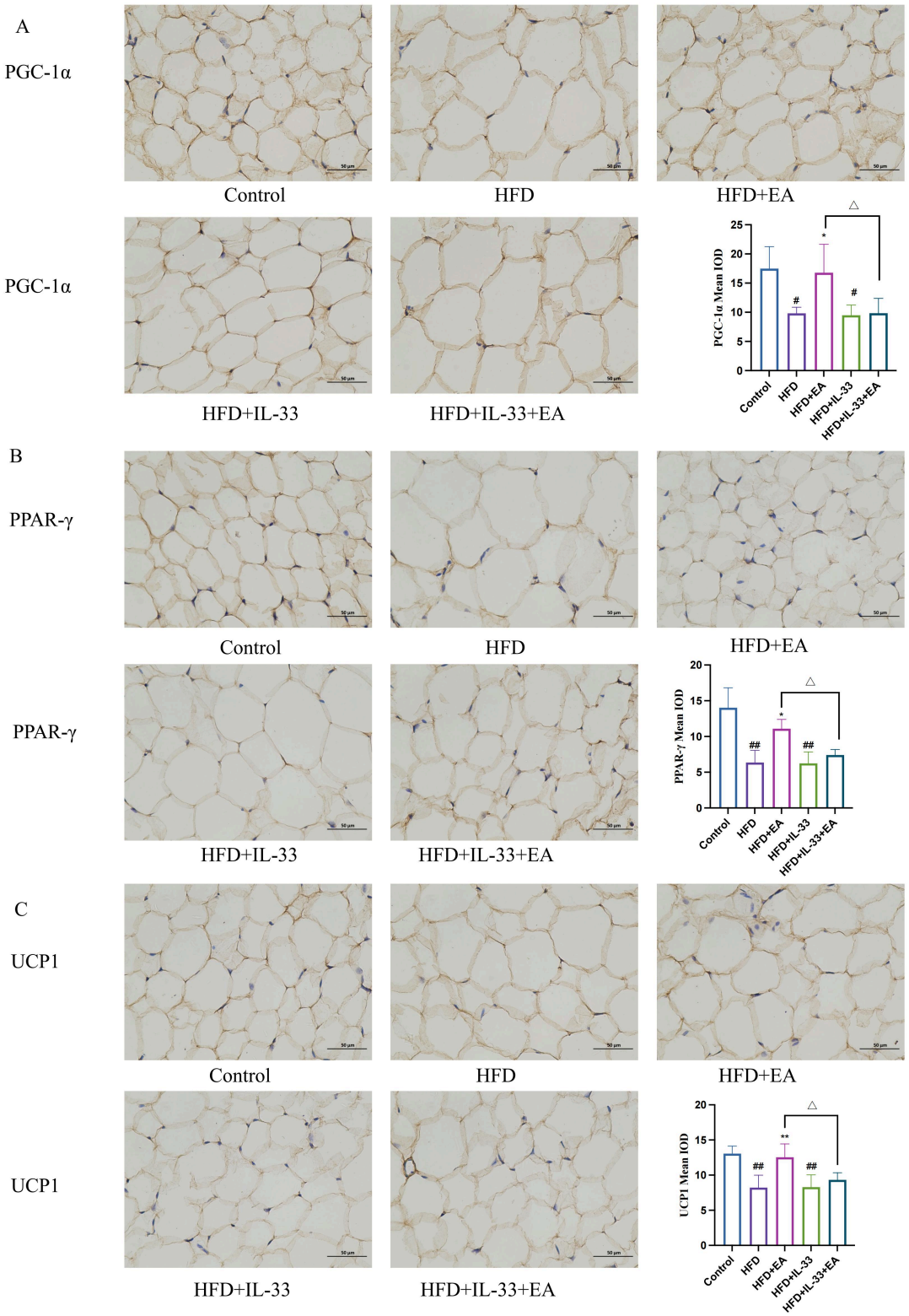


Figure 8

8 IL-33 Mediates EA-Induced Thermogenic protein Upregulation. (A-C) Expression of PGC-1α, PPAR-γ and UCP1 evaluated by immunohistochemical. $^{\#}P < 0.05$, $^{\#\#}P < 0.01$ vs. the control group. $^{*}P < 0.05$, $^{**}P < 0.01$ vs. the HFD group; $^{\triangle}P < 0.05$, $^{\triangle\triangle}P < 0.01$, vs. the HFD+EA group (n=5).

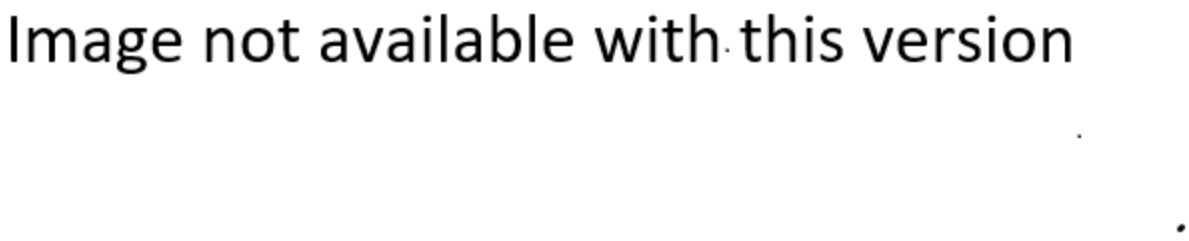


Figure 9

EA alleviates obesity in mice by activating IL-33/ST2 signaling to regulate ILC2 function and gut microbiota.

Supplementary Files

This is a list of supplementary files associated with this preprint. Click to download.

- GraphicalAbstract.jpg